Geophysical Research Letters

RESEARCH LETTER
10.1029/2021GL094367

Simulated Global Coastal Ecosystem Responses to a Half-Century Increase in River Nitrogen Loads

Xiao Liu[1,2], Charles A. Stock[2], John P. Dunne[2], Minjin Lee[1,2], Elena Shevliakova[2], Sergey Malyshev[2], and Paul C. D. Milly[3]

[1]Atmospheric and Oceanic Sciences, Princeton University, Princeton, NJ, USA, [2]NOAA/OAR Geophysical Fluid Dynamics Laboratory, Princeton, NJ, USA, [3]U.S. Geological Survey, Princeton, NJ, USA

Key Points:

- Coastal ecosystem responses to long-term changes in river nitrogen (N) loads are simulated using a global ocean biogeochemical model
- Increasing river N loads are linked to elevated N inventory, primary production, and benthic detrital flux in the global coastal ocean
- Residence time and N limitation state are important factors driving comparative coastal ecosystem susceptibility to enhanced N loads

Supporting Information:

Supporting Information may be found in the online version of this article.

Correspondence to:

X. Liu,
xiao.liu@noaa.gov

Citation:

Liu, X., Stock, C. A., Dunne, J. P., Lee, M., Shevliakova, E., Malyshev, S., & Milly, P. C. D. (2021). Simulated global coastal ecosystem responses to a half-century increase in river nitrogen loads. *Geophysical Research Letters*, *48*, e2021GL094367. https://doi.org/10.1029/2021GL094367

Received 21 MAY 2021
Accepted 9 AUG 2021

Abstract Coastal ecosystems are increasingly threatened by anthropogenic stressors such as harmful algal blooms and hypoxia through the combined effects of eutrophication and warming. As a major terrestrial nitrogen source to the ocean, rivers play a key role in shaping coastal nitrogen budgets and biogeochemical cycling. Combining an enhanced-resolution, global ocean biogeochemical model with temporally changing river inputs, we estimate that elevated river nitrogen loads alone resulted in a 5.8% increase (16.6 Tg) in the global coastal nitrogen inventory from 1961 to 2010, accompanied by increases in coastal net primary productivity (+4.6%) and benthic detrital flux (+7.3%). The ecosystems most sensitive to added nitrogen were those with long residence times and strong nitrogen limitation. While even enhanced-resolution global models remain limited in their capacity to resolve shelf-scale responses, these basic factors provide two relevant axes for frameworks assessing the comparative coastal ecosystem susceptibility to enhanced nitrogen loads, and the effectiveness of mitigation strategies.

Plain Language Summary Over the past century, human activities have resulted in substantial global changes that threaten the stability and functionality of coastal habitats. One of these impacts was through nutrient pollution of river runoffs, which have triggered harmful algal blooms and caused low-oxygen conditions in many coastal regions. However, it is challenging for models to simulate coastal impacts of increasing river nutrient loads, especially on a global scale and over a long period of time. Here we take advantage of some recent modeling advances to provide a global perspective on coastal ecosystem responses to increasing river nitrogen loads over the half-century between 1961 and 2010. Overall, we show that the global coastal ocean accumulated more nitrogen over time as river nitrogen loads increased. This caused the primary production of the global coastal system (i.e., the conversion of inorganic to organic materials through photosynthesis) to increase as well. However, we found that the sensitivity of each coastal ecosystem to comparable changes in nitrogen loads varied considerably. This variability was to a large extent related to two factors: the rate of exchange between coastal waters and the adjacent ocean waters, and whether nutrients are limited for phytoplankton to conduct photosynthesis in that system.

1. Introduction

Despite covering less than 8% of the global ocean, the coastal ocean (here defined by the 200 m isobath) provides essential ecosystem services by hosting an abundant and diverse array of marine life and supporting the vast majority of global fish catch (Lotze et al., 2006; Pauly & Zeller, 2016). The removal and transformations of river nutrients and other constituents during transport from the coasts to the open ocean are central to coastal ecosystems, and both regional and global biogeochemical cycles (Cai, 2011). Over the past century, anthropogenic activities have resulted in substantially elevated fertilizer use and climatic changes (Bouwman et al., 2013; IPCC, 2019), leading to alterations to coastal environments often manifested as eutrophication, acidification, and deoxygenation (Doney, 2010; Gilbert et al., 2010; Orr et al., 2005). These stressors may exacerbate one another, together altering coastal and global carbon and nutrient budgets (Bauer et al., 2013; Regnier et al., 2013) and potentially threatening coastal populations and economies (Lotze et al., 2006; Worm et al., 2006).

Over recent decades, anthropogenic eutrophication has become a major threat to the health of coastal ecosystems, responsible for harmful algal blooms, reductions in water clarity, and the expansion of low-oxygen

"dead zones" in many regions (Diaz & Rosenberg, 2008; Gilbert et al., 2010; Paerl et al., 2018). As a primary cause for eutrophication, rivers have supplied a substantial and sharply increasing amount of anthropogenic nitrogen to the world's coastal ocean. Bouwman et al. (2006) used a global terrestrial and hydrological model to estimate that export of total nitrogen from rivers to the ocean increased by 29% from 1970 (33.9 Tg yr^{-1}) to 1995 (43.7 yr^{-1}). Also using a global modeling approach, Lee et al. (2019) suggested that river loads of dissolved nitrogen increased by 52% from the early 1940s (25.2 Tg yr^{-1}) to 2010 (38.9 Tg yr^{-1}), while Seitzinger et al. (2010) suggested a similar rate of increase in dissolved nitrogen loads over the past decades (about 30% from 1970 to 2000). These nitrogen species, along with other river constituents, are subject to some complex transformation and removal processes in coastal waters and sediments (e.g., photosynthesis, remineralization, denitrification, and burial; Middelburg et al., 1996, 2007; Seitzinger et al., 2002, 2006). These processes determine not only the coastal imprints but also the transport of river materials across the open ocean boundaries, thus contributing to changes in larger-scale biogeochemical cycling (Cai, 2011; Herbert, 1999; Najjar et al., 2018; Voss et al., 2013).

Decades of research has been dedicated to investigating ecosystem responses to anthropogenic perturbations in coastal nutrient budgets (e.g., Dagg & Breed, 2003; Fennel & Laurent, 2018; Liu et al., 2005). Although these studies focused primarily at regional scales, more recent efforts have provided cross-system syntheses on coastal ecosystem sensitivity to nutrient perturbations. For example, Fennel and Testa (2019) revealed differential controlling factors (e.g., river nutrient loads, coastal upwelling of low-oxygen waters) underlying hypoxia generation across diverse coastal systems, and associated persistent hypoxic conditions to longer water residence time. Blaas and Kroeze (2016) derived a "eutrophication potential indicator" that compares nitrogen and phosphorus loads to the Redfield ratios expressing local requirements of diatom growth, suggesting that 38 out of the 48 studied large rivers in Europe had a high potential to cause coastal eutrophication. Quantifying and characterizing the global scale coastal responses to riverine perturbations has proven more challenging. Global coastal zones border over 500,000 kilometers of coastline, stretching from pole-to-pole, and consist of over 100 million km^2 of complex bathymetry and diverse hydrological and biogeochemical conditions (Holt et al., 2017). The scale of coastal environments and the complex underlying processes challenge observation-based analysis in even the most well-monitored systems. While combining numerical models with available observations has proven an effective strategy for individual coastal ecosystems (Cahill et al., 2016; de Mutsert et al., 2016; Fennel et al., 2008; Friedrichs et al., 2019), global syntheses are hindered by coarse horizontal resolutions of current-generation global models necessitated by computational constraints.

Here, we take advantage of a number of recent modeling advances to provide a global perspective on coastal ecosystem responses to increasing river nitrogen loads over the half-century period between 1961 and 2010. We combine an enhanced-resolution (at nominal 0.25° or approximately 25 km), global ocean physical-biogeochemical model with dynamic (i.e., temporally changing) river freshwater and nitrogen fluxes derived from a global land biosphere model (Lee et al., 2019). We assess simulated changes across the coastal portions (shallower than 200 m) of 66 globally distributed Large Marine Ecosystems (https://www.lmehub.net), hereafter referred to as cLMEs. This analysis suggests a widespread response of coastal ecosystems to increasing river nitrogen loads. The sensitivity of each ecosystem to comparable changes in nitrogen loads per area, however, varied considerably, and was associated to contrasts in coastal residence time and nutrient limitation state of the system. These basic sensitivity factors provide two relevant axes for frameworks assessing the comparative susceptibility of globally distributed coastal ecosystems to enhanced nitrogen loads, and the effectiveness of mitigation strategies.

2. Methods

2.1. The Coupled, Global Ocean Physical-Biogeochemical Model

The ocean physical model used in this study was configured from the 6th generation of the Modular Ocean Model (MOM6) and its accompanying 2nd generation Sea Ice Simulator (SIS2) both developed at the NOAA Geophysical Fluid Dynamics Laboratory (Adcroft et al., 2019). The model grid used in our simulations has a nominal horizontal resolution of 0.25° or approximately 25 km. Previous work has shown that, on a global scale, key physical contrasts in coastal ocean properties such as residence times and salinity gradients are reasonably represented at this resolution (Liu et al., 2019).

The ocean physical model was integrated with GFDL's Carbon, Ocean Biogeochemistry and Lower Trophics ocean biogeochemical model version 2 (COBALTv2; Stock et al., 2020). The 33-tracer COBALTv2 model simulates global scale dynamics of carbon, nitrogen, phosphorus, iron, and oxygen, along with three explicit phytoplankton (small, large, and N_2-fixing) groups and three explicit zooplankton groups by size. COBALTv2 has been evaluated extensively at global and basin scales (Stock et al., 2020), and we further note that the improved representation of river fluxes herein has ameliorated the over-expression of phosphate limitation in prior simulations (Figure S1). Comparisons of simulation results with observed nitrate (WOA18; Garcia et al., 2018; Figure S2) and satellite-based chlorophyll and primary production estimates (Copernicus-GlobColour CHL_1 and PP; Antoine & Morel, 1996; Maritorena et al., 2010; Figures S3 and S4) show that the simulation captured the primary contrasts in these quantities across globally distributed cLMEs ($r = 0.88$, 0.65, and 0.60, respectively). The simulation is limited, however, in its ability to represent the full range of chlorophyll across the coastal ocean, particularly nearshore areas of the highest satellite-based chlorophyll (Figure S3). This limitation is shared with other global and regionally applied ecosystem models (e.g., Friedrichs et al., 2007; Stock et al., 2017; Van Oostende et al., 2018). Furthermore, we recognize that the accuracy of global observational products enlisted for comparisons in Figures S2–S4 may be challenged by filtering (WOA18 v2 nitrate, 1° grid) and the optical complexity of nearshore waters (Chl and PP, Schofield et al., 2004). The potential implications of these limitations for our model results, and potential improvements for future efforts, will be discussed in Section 4.

2.2. The Dynamic River Inputs Simulated by a Land Biosphere Model

The dynamic (i.e., temporally changing) river freshwater and nitrogen fluxes are simulated by GFDL's land-watershed model LM3-TAN (Land Model version 3 with Terrestrial and Aquatic Nitrogen) (Lee et al., 2014, 2019), which incorporates a global river routing and lake model (Milly et al., 2014) into a terrestrial ecosystem model (Gerber et al., 2010; Shevliakova et al., 2009) to simulate nitrogen storage and cycling processes both in the terrestrial environment and in rivers. The land model simulation reported in Lee et al. (2019) provides monthly varying fluxes of freshwater and dissolved nitrogen (in both inorganic and organic forms: DIN and DON) from more than 2000 river discharge points along the global coasts since the preindustrial period (Text S1, Figures S5 and S6). The elevated nitrogen loads detected from this data set were primarily due to an increase in nitrogen concentration rather than freshwater (Figure S5). To estimate river fluxes of particulate nitrogen (PN), dissolved inorganic and organic phosphorus (DIP, DOP), and particulate phosphorus (PP) for the ocean model, we assessed the Global Nutrient Export from WaterSheds (NEWS) database (Seitzinger et al., 2005) and analyzed the NEWS reported ratio of PN, DIP, DOP, or PP to the total dissolved nitrogen (DN = DIN + DON) at each river discharge point simulated by the LM3-TAN model. We then applied these ratios to the simulated DN flux to obtain PN, DIP, DOP, and PP fluxes accordingly (see Text S2 for more details). DON and DOP in the river inputs were fractionated to the labile (40%), semi-labile (30%), and semi-refractory (30%) pools, consistent with the range of bioavailability found by Wiegner et al. (2006).

2.3. Ocean Model Simulations

The coupled MOM6-COBALTv2 ocean model was initialized at rest using long-term climatologies of observed temperature (Locarnini et al., 2013), salinity (Zweng et al., 2013), oxygen (Garcia et al., 2014a), nitrate, phosphate, and silicate (Garcia et al., 2014b) from the World Ocean Atlas (WOA 2013v2), and preindustrial dissolved inorganic carbon and total alkalinity from the GLobal Ocean Data Analysis Project (GLODAPv2) (Olsen et al., 2016). The simulation was spun up for a total of 208 years with eight repeating cycles of 26 years between 1959 and 1984 forced by the Japanese 55-year Reanalysis (JRA-55) products (Tsujino et al., 2018), from which two experiments (*dynRN* and *climRN*, see below) were initialized and run for 52 years from 1959 to 2010. During the last spin-up cycle, climatological values of river freshwater runoff and nutrient (DIN, DON, PN, PIN, PON, and PP) concentrations averaged over the period just prior to the experiment initialization (1951–1958) were used. The *dynRN* experiment was forced with both dynamic atmospheric states (6-hourly JRA-55 reanalysis) and dynamic river freshwater and nutrient fluxes from LM3-TAN (described in Section 2.2), while *climRN* was forced with the same dynamic atmospheric states but river fluxes were held at the 1951–1958 climatological values consistent with the spin-up simulation.

River fluxes of dissolved inorganic carbon and alkalinity were calibrated to match carbon burial and net alkalinity losses to the sediment following Dunne et al. (2012). Concentrations of these constituents, as well as of iron and mineral particles, were held constant in both experiments. The spatially variant, atmospheric deposition fluxes of nitrogen were derived from simulated results for Year 1990 (Horowitz, 2006), which were also held constant over time in both experiments. Thus, contrasting the results of *dynRN* and *climRN* provided a way to isolate the responses of coastal biogeochemical and ecosystem states to long-term riverine perturbations, and also to minimize the effects of model drift on simulated responses.

2.4. Model Analyses

As mentioned in Section 1, we focus on the coastal portions of globally distributed Large Marine Ecosystems (cLMEs) to assess global and regional variability of river loads, coastal nitrogen budgets, and ecosystem responses. Specifically, global coastal nitrogen budgets were computed for all coastal grid cells (<200 m) of the model domain, including the 66 cLMEs as well as shallow waters not identified as part of a cLME. For regional analyses, we excluded the heavily ice-covered Arctic (cLME #61) and Antarctic regions (#64), the semi-enclosed Black Sea (#62), and the Hawaiian Islands system (#10) which is composed of few cLME grid cells. Text S2 provides a detailed description of how each coastal nitrogen budget term was defined and computed. Comparing *climRN* with the last spin-up cycle where identical forcings were used, we show that simulated magnitudes of coastal nitrogen budgets were minimally affected by model drift over the experiment period. We further note that model drift caused a small decline in global Coastal Nitrogen Inventory (CNI), suggesting that the simulated increasing CNI trend associated with riverine fluxes (Section 3.1) was not an effect of model drift (Text S3, Figure S7).

In the results below, we first report the mean terms and half-century (between 1961 and 2010) changes of coastal nitrogen budgets based on *dynRN* (Section 3.1, Figure 1). We then assess coastal nitrogen budget changes originating solely from riverine perturbations based on patterns and trends revealed by contrasting *dynRN* and *climRN* (Sections 3.2 and 3.3, Figures 2–5). In additional to coastal nitrogen budgets, we consider changes in two ecosystem response measures with high relevance to riverine perturbations: net primary production (NPP) and the flux of organic materials to the benthos (i.e., benthic detrital flux, or BDF). The former quantifies the stimulation of net carbon fixation of relevance to algal blooms and the total heterotrophic respiratory demand shaping oxygen and carbon budgets. The latter provides a measure of enhanced supply of organic material to the benthos where subsequent aerobic respiration may contribute to benthic hypoxia, or where denitrification/burial could remove nitrogen from the system.

Finally, two coastal ocean properties were analyzed to provide mechanistic insights for factors governing the comparative sensitivity of coastal nitrogen budgets and ecosystem responses to riverine perturbations: (a) coastal residence time and (b) nitrogen (NO_3 and NH_4) limitation state for photosynthetic growth. Coastal residence time for each system was estimated following Liu et al. (2019) based on an idealized "coastal age" tracer implemented in the model (see Text S4 and Figure S8 for more details). Nitrogen limitation state is quantified as $(1-\gamma)$, where γ is the ratio between nitrogen-limited and nitrogen-saturated growth rate after considering light and temperature limitation. A higher value of $(1-\gamma)$ thus indicates a stronger nitrogen limitation on photosynthetic growth in the system. Before assessing the effects of these factors on the sensitivity of each cLME to comparative river nitrogen loads, changes in nitrogen loads were normalized by the area of each cLME to provide a consistent measure of nitrogen enrichment intensity (i.e., g N m^{-2} yr^{-1}).

3. Results

3.1. Coastal Nitrogen Budgets and Total Inventory Change (1961–2010)

The half-century of 1961–2010 witnessed a substantial increase in both the magnitudes of river nitrogen loads and their fractional contributions to total nitrogen inputs to the global coastal ocean (Figures 1a, 1b, S5, and S6). Annual loads of both DIN and TON increased significantly ($p < 0.05$) over this period, changing from a total of 42.7–56.6 Tg N yr^{-1}. River inputs thus accounted for just 37% of the total coastal nitrogen source in the 1960s, but 47% by the turn of the century. Increases in river nitrogen loads contrasted with a relatively constant net supply of DIN from the open ocean (47.4 Tg yr^{-1} or 41%; Figures 1a and 1b). Contributions from N_2 fixation (TON, 15.4 Tg yr^{-1} or 13%) and atmospheric deposition (DIN, 4.5 Tg yr^{-1} or

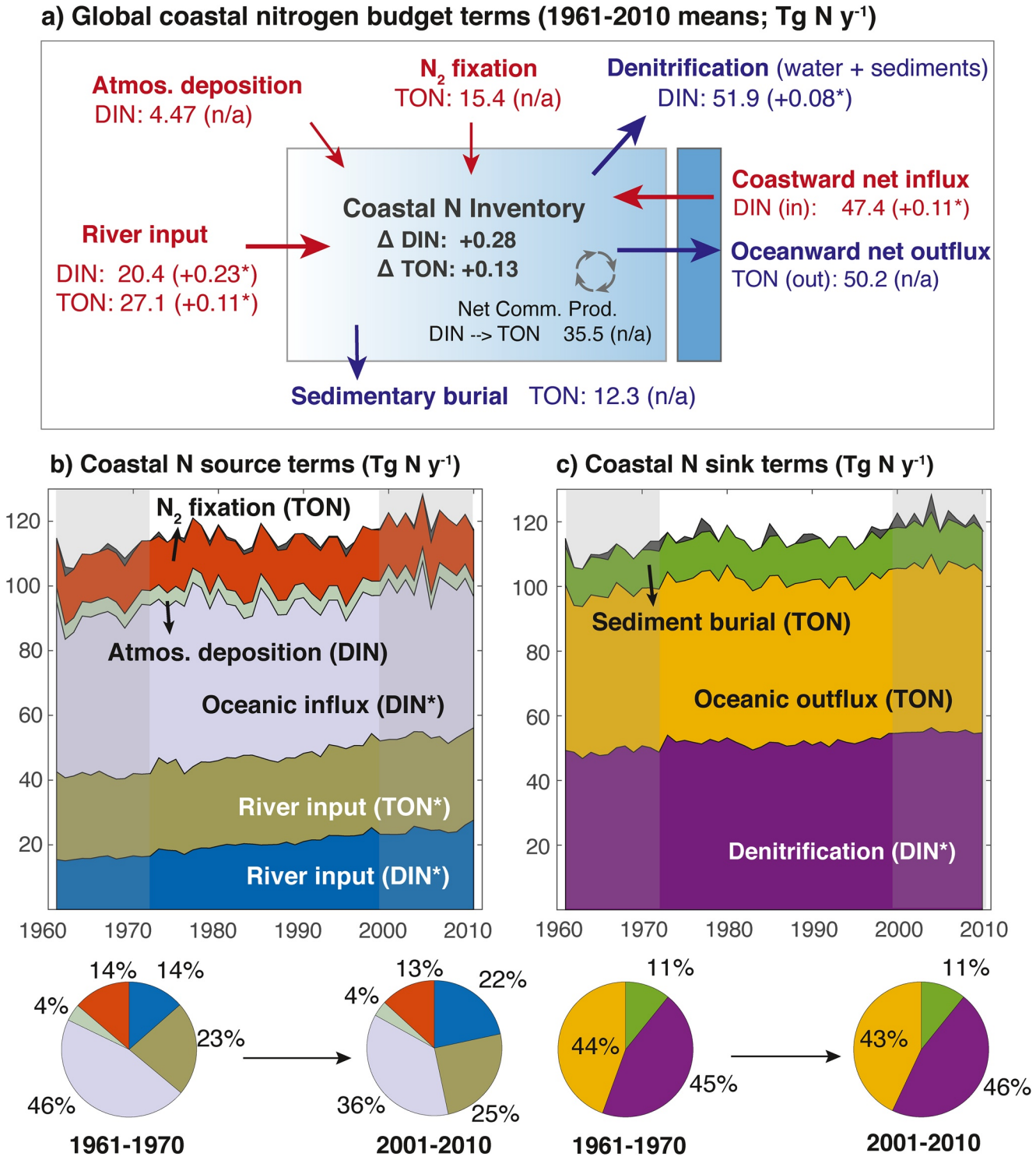

Figure 1. (a) Simulated global coastal nitrogen budget terms averaged over the 50-year period between 1961 and 2010. These terms were computed for the entire global coastal ocean (light blue box), which is separated from the open ocean (dark blue box) by the 200 m isobath. Numbers in the parentheses show calculated regression slopes, indicating average rates of change (Tg N yr^{-1}). Stars (*) are used to identify budget terms of which annual means displayed a significant increasing trend ($p < 0.05$) during the simulation period, while n/a indicates otherwise. Nitrogen source terms (panel b) and sink terms (panel c) include both inorganic (DIN, dissolved inorganic nitrogen) and organic (TON, total dissolved and particulate organic nitrogen) forms. Note that the thin black polygons at the top of the bar charts in (panels b and c) reflect net changes in coastal nitrogen inventory, with negative changes plotted as source terms and positive changes plotted as sink terms. Pie charts at the bottom show the fractional contribution of each budget term to total nitrogen source or sink during the first (1961–1970) and last decade (2001–2010) of the simulation period (highlighted in gray shade in [panels b and c]).

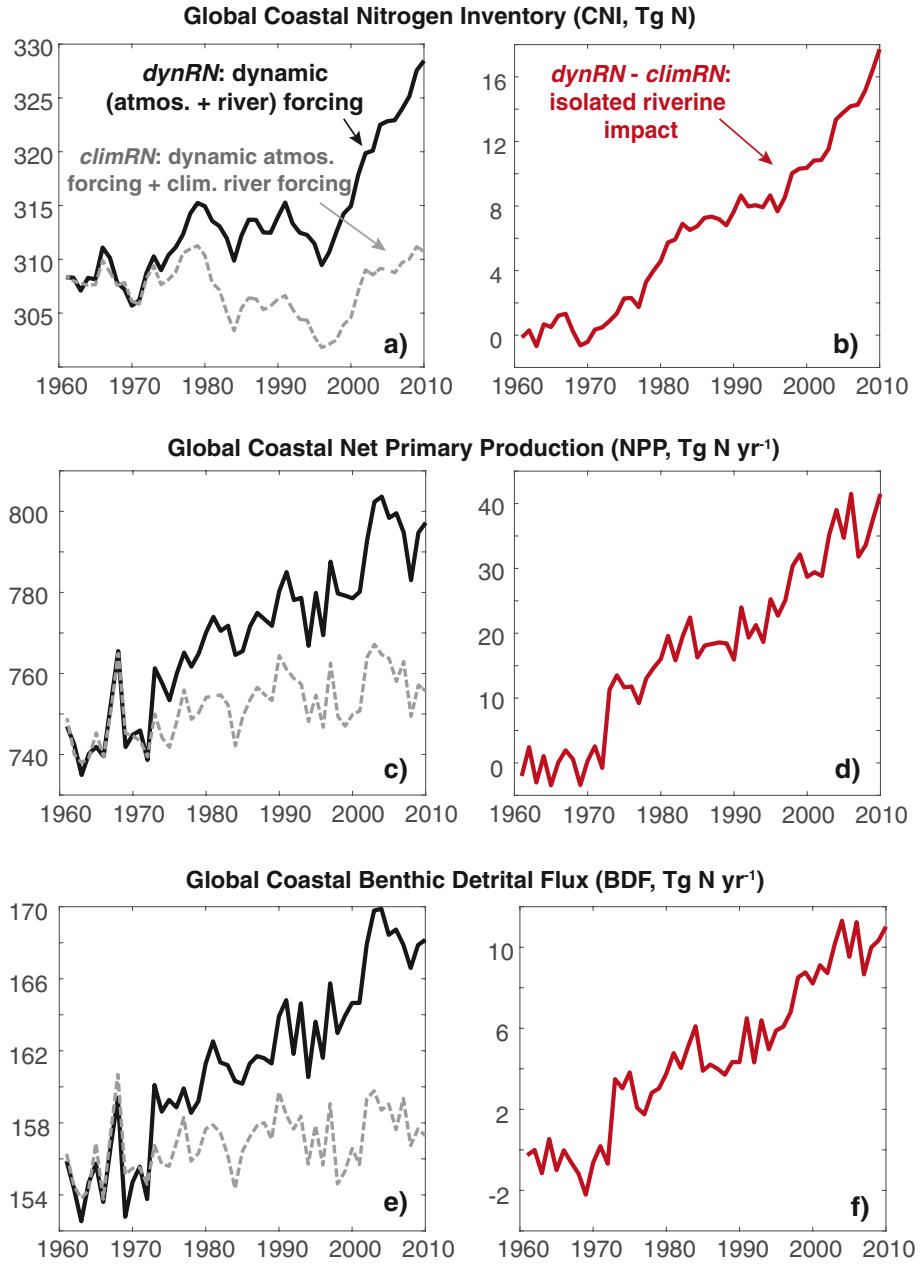

Figure 2. Long-term changes in Global coastal nitrogen inventory (CNI, panel [a]), global coastal net primary production (NPP, in nitrogen units, panel [c]), and global coastal benthic detrital flux (BDF, in nitrogen units, panel [e]) over the 50-year simulation period between 1961 and 2010. All three quantities showed a significant increasing trend ($p < 0.05$) in *dynRN* with dynamic river freshwater and nutrient fluxes (solid black line). A significant increasing trend ($p < 0.05$) of a much smaller magnitude was also observed for NPP, but not for CNI and BDF, in *climRN* (dashed gray line), where the dynamic riverine fluxes were replaced by 1951–58 climatologies. The riverine impacts (solid red line) on long-term changes in CNI (panel b), NPP (panel d), and BDF (panel f) were isolated by subtracting the *climRN* signal from *dynRN* (see Section 2.3), thus removing the effects of atmospheric variability and model drift in the control simulation. The increasing trends associated with riverine forcing were significant for all three quantities ($p < 0.05$).

4%) were significantly less than those of the riverine and oceanic origins. Coastal nitrogen losses comprised nearly equal contributions from oceanward net transport of TON (50.2 Tg yr^{-1} or 44%) and denitrification processes in the water column and sediments (51.9 Tg yr^{-1} or 45%), as well as a small fraction from sedimentary burial of detritus (12.3 Tg yr^{-1} or 11%). Net oceanic TON export reflected a substantial net transformation of inorganic nitrogen to longer-lived organic forms within coastal ecosystems (NCP = 35.5 Tg yr^{-1}),

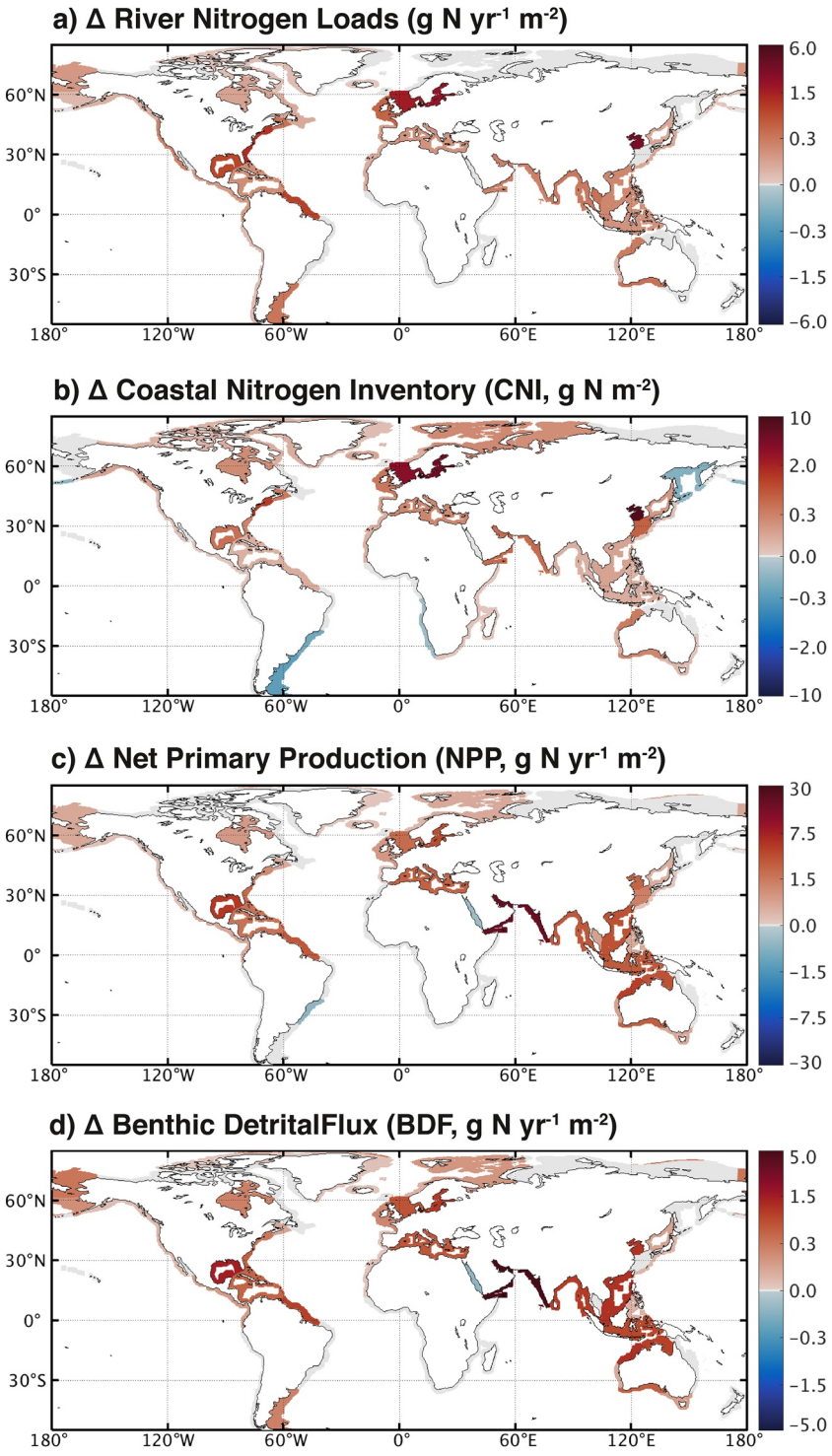

Figure 3. Area-normalized changes in river nitrogen loads, coastal nitrogen inventory (CNI), net primary production (NPP, in nitrogen unit), and benthic detrital flux (BDF, in nitrogen unit) in globally distributed cLMEs averaged between 1961 and 2010. Regression slopes were derived based on trends detected by contrasting *dynRN* and *climRN* experiments. cLME-scale changes shown here were calculated only from significant trends ($p < 0.05$) by multiplying regression slope with simulation period (50 years). Gray color indicates an insignificant or negligible change.

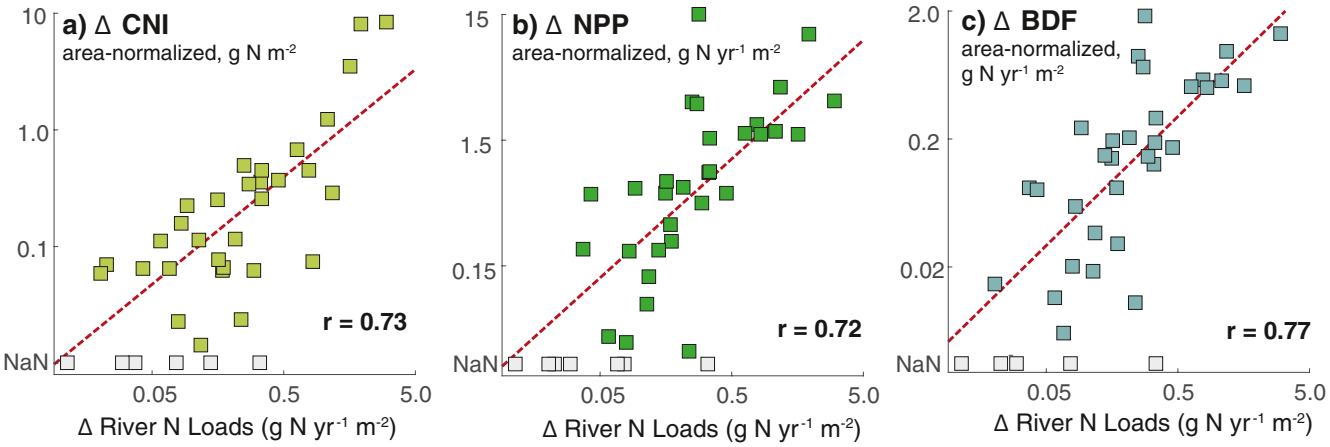

Figure 4. Area-normalized changes in coastal nitrogen inventory (CNI), net primary production (NPP, in nitrogen unit), and benthic detrital flux (BDF, in nitrogen unit) and their relationships with Area-normalized changes in river nitrogen loads in globally distributed cLME averaged between 1961 and 2010. Results are shown only for the cLMEs where a significant increasing trend ($p < 0.05$) in river nitrogen loads was detected. The colored squares denote cLMEs where both the ecosystem response variable and the river nitrogen loads displayed significant increasing trends over the simulation period, while the light gray squares denote cLMEs where only the river nitrogen loads displayed a significant increasing trend but not the ecosystem state. These data points (light gray squares) were not considered in the regression analysis. The dashed lines reflect a best-fit linear regression between each pair of variables. Note that, in this analysis, all quantities were area-normalized to provide a common measure of nitrogen load intensity and ecosystem sensitivity.

consistent with regional findings (e.g., Feng et al., 2015; Friedrichs et al., 2019). Unlike nitrogen sources, the fractional contribution of each sink term to the total coastal nitrogen sink remained relatively constant over the 50-year simulation period (Figures 1a and 1c, refer to pie charts).

The differential long-term changes in nitrogen source and sink terms described in Figure 1 resulted in an overall net increase in the global CNI (defined as the total amount of nitrogen in coastal waters in both

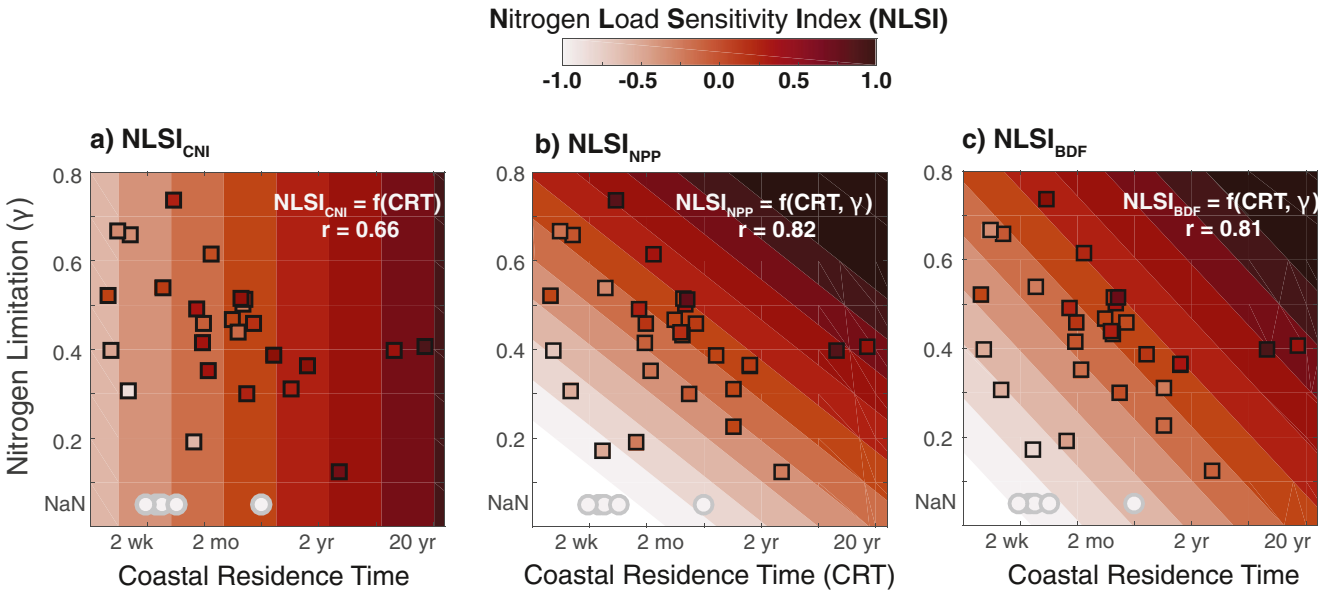

Figure 5. Nitrogen Load Sensitivity Index (NLSI, color-coded) calculated for (a) coastal nitrogen inventory (CNI), (b) net primary production (NPP), and (c) benthic detrital flux (BDF) in globally distributed cLMEs. Results are shown only for the cLMEs where a significant increasing trend in river nitrogen loads was detected. NLSI for each ecosystem state is plotted in the space of coastal residence time (CRT) and the nitrogen limitation state (γ) for each cLME. The regression analysis shows that NLSI for CNI is a function of CRT ($p < 0.05$), while NLSI for NPP and BDF is a function of both CRT and γ ($p < 0.05$). The colored squares denote the cLMEs where both the ecosystem variable and the river nitrogen loads showed significant increasing trends between 1961 and 2010. The light gray circles denote the cLMEs where nitrogen is not the most limiting element compared to phosphorus and iron. These data points were not included in the regression analysis.

dissolved and particulate forms), with an average accumulation rate of 0.41 Tg yr^{-1}. While modest on a yearly basis, this accumulation translated into a total increase of 20.5 Tg (+6.7%) over the 50-year simulation period. The long-term global CNI gain was characterized by an initial moderate increase between 1961 and 1995, followed by an accelerated increase from 1996 to 2010 (*dynRN* shown as the solid black line in Figure 2a). A marked CNI increase during this latter period, however, was also seen in *climRN*, where river nitrogen concentrations were held as constants and only atmospheric forcing changed (dashed gray line in Figure 2a). This suggests that the rapid coastal nitrogen accumulation between 1996 and 2010 was a combined effect of riverine and atmospheric forcing driven variability. Subtracting *climRN* from *dynRN* isolates the riverine effect (Section 3.2), revealing a steadier CNI increase over this half-century period.

3.2. Global Scale and Regional Coastal Responses to Increasing River Nitrogen Loads

Long-term changes in river nitrogen loads resulted in widespread coastal increases in CNI (Figures 2a, 2b and 3b), NPP (Figures 2c, 2d and 3c), and BDF (Figures 2e, 2f and 3d). It was estimated that, on a global scale, elevated river nitrogen loads alone resulted in an increase of 16.6 Tg in CNI (+5.8%, $p < 0.05$ for regression slope, Figure 2b) over the 50-year simulation. This accumulation of coastal nitrogen was accompanied by increases in global coastal NPP (+41.2 Tg N yr^{-1} or +4.6%, $p < 0.05$; Figure 2d) and BDF (+11.4 Tg N yr^{-1} or +7.3%, $p < 0.05$; Figure 2e). Averaged over all coastal areas, this corresponds to an NPP increase of 0.45 g N m^{-2} yr^{-1} and a BDF increase of 0.13 g N m^{-2} yr^{-1}. Significant increasing trends in regional CNI were detected in 31 of the 62 coastal systems assessed (51% by area; Figure 3b), with 27 systems also exhibiting significant increases in both NPP and BDF (42% by area; Figures 3c and 3d). Some coastal systems showed a particularly strong response, such as those in Southeast Asia, Europe, Central America, and the Arabian Sea. These regions are also consistently among those receiving rapidly increasing anthropogenic nitrogen inputs into their river basins (e.g., through fertilizer use and/or atmospheric deposition, Green et al., 2004; Lu & Tian, 2017) and many have experienced adverse impacts from coastal eutrophication (e.g., the Baltic Sea, Murray et al., 2019; the Yellow Sea, Zhang et al., 2019).

3.3. Comparative Coastal Ecosystem Sensitivity to River Nitrogen Loads

We analyzed the general relationships between changes in river nitrogen loads and responses of CNI, NPP, and BDF across 62 cLMEs. After normalizing river loads by the cLME area to provide a common measure of nitrogen load intensity (g N yr^{-1} m^{-2}), high correlations were evident between changes in river nitrogen loads and responses of all three ecosystem quantities (Figure 4, $r = 0.73$ for CNI, $r = 0.72$ for NPP, and $r = 0.77$ for BDF). To first order, the magnitude of coastal ecosystem responses scaled with added river nitrogen per unit area. The residuals around these global mean relationships, however, were substantial. To quantify the comparative sensitivity across these diverse coastal ecosystems, we define an "*Nitrogen Load Sensitivity Index*" (NLSI) based on the residuals around the relationships in Figure 4 to quantify the regional departure of each system from the global mean ecosystem responses. We consider the *sensitivity* of an ecosystem state to river nitrogen load perturbations as the magnitude of long-term change in that state scaled by the magnitude of long-term change in river nitrogen loads per unit area. Specifically:

$$\mathrm{NLSI}_{E,i} = \log_{10}\left(\Delta E_i\right) - \overline{R}_{E,i} \tag{1}$$

$$\overline{R}_{E,i} = a * \log_{10}\left(\Delta N_i\right) + b \tag{2}$$

where ΔE_i is the area-normalized long-term change of an ecosystem state E (e.g., CNI, NPP, or BDF) in a coastal system i, and $\overline{R}_{E,i}$ is the global mean response of state E as a linear function of ΔN_i. Thus, a large positive (negative) NLSI indicates a high sensitivity of an ecosystem state to a comparable increase in river nitrogen loads, that is, the system sits above (below) the dashed line in Figure 4 that characterizes the mean response to a given nitrogen load increase per unit area.

NLSI ranged from −0.98 to 0.95 for CNI, −0.81 to 0.79 for NPP, and −0.74 to 0.76 for BDF across the 37 coastal systems that experienced significant ($p < 0.05$) increasing trends in river nitrogen loads (Figure 5). Because the NLSI was calculated after $\log_{10}$-transformation (Equations 1 and 2), this range corresponded to an order of magnitude differential ecosystem response for the same addition of riverine nitrogen per unit

area. For example, the half-century increase in NPP on the Northwest Australian Shelf (5.9 g N m^{-2} yr^{-1}; $NLSI_{NPP} = 0.79$) was 6.2 times the response to an increase of 0.28 g N m^{-2} yr^{-1} in river nitrogen loads expected from the regression across all coastal systems, while the NPP response in the Kuroshio Current system (0.08 g N m^{-2} yr^{-1}; $NLSI_{NPP} = -0.81$) was only 0.15 of the global mean response to a similar increase of nitrogen loads in that system of 0.23 g N m^{-2} yr^{-1}.

We found that a significant fraction of the NLSI variability could be explained by the differential residence time and/or nitrogen limitation state across these diverse coastal systems (Figure 5).Residence time, for example, ranging from several days to more than 10 years (Liu et al., 2019), explained about 44% of the variability in $NLSI_{CNI}$ (Figure 5a, $r = 0.66$). This suggests that, as nitrogen inputs increase, the more retentive coastal systems tend to accumulate more nitrogen than those experiencing rapid exchanges with the open ocean. A longer residence time also led to a more marked ecosystem response, as reflected in positive relationships with residence time for $NLSI_{NPP}$ and $NLSI_{BDF}$. These latter responses, however, were also shaped by the baseline nitrogen limitation state in that system. In other words, NPP and BDF in a strongly nitrogen-limited system tends to increase more markedly in response to a given increase in nitrogen loads, compared to a system that is less nitrogen-limited. A bi-factorial correlation analysis shows that 66% and 65% of the variability in $NLSI_{NPP}$ and $NLSI_{BDF}$, respectively, could be explained by the combined effects of varying residence time and nitrogen limitation state across these cLMEs (Figure 5b, $r = 0.82$, Figure 5c, $r = 0.81$).

4. Discussion

Coastal eutrophication has become a rising global problem over the past decades and, together with other coastal stresses, has impacted the structure of coastal ecosystems, human health, and coastal economies (e.g., Rabalais et al., 2009). Actions to mitigate eutrophication and reverse its impact are underway in many regions. However, an effective strategy for nutrient reduction requires an improved understanding of future changes in nutrient sources as well as the comparative sensitivity of each coastal ecosystem to added nutrients. Our analyses suggest that, although the degree of coastal eutrophication (i.e., increased nitrogen load per unit area and nitrogen accumulation rate) and its impacts on coastal ecosystems (i.e., changes in primary productivity and benthic detrital flux) were well correlated on a global scale, there existed a considerable range of sensitivity across diverse ecosystems. We attributed a large part of this differential sensitivity to two coastal ocean properties: residence time and nitrogen limitation state. Residence time is a fundamental property of coastal systems, providing a time-scale for the complex coastal biogeochemical processes to impart their unique signatures on ecosystem responses (Liu et al., 2019). Global scale syntheses of shelf-scale residence times have been done based on theoretical and empirical scaling arguments (Sharples et al., 2017), idealized numerical experiments (Izett & Fennel, 2018), and global ocean models (Bourgeois et al., 2016; Liu et al., 2019; see Text S4 for more details). Previous work has shown that coastal retention might play an important role in the generation and development of coastal stressors, such as harmful algal blooms and hypoxia (e.g., Fennel & Laurent, 2018; Fennel & Testa, 2019; Pitcher et al., 2010). Assuming sufficient contact with source waters (i.e., long-enough residence time), phytoplankton growth and primary productivity are controlled by the most limiting factor in the system among temperature, light, and nutrients (Cloern, 1999; Howarth et al., 1988). In most coastal ecosystems, nitrogen is considered the primary limiting nutrient and a major cause of eutrophication (Howarth & Marino, 2006). *In situ* enrichment experiments have shown that the rate of phytoplankton growth can be tightly coupled to nitrogen supply, but only when ambient nitrogen is low (Teichberg et al., 2010). Our analyses consider both residence time and nitrogen limitation, suggesting that the rate of coastal nitrogen accumulation per area is primarily attributed to long residence time, while rates of ecosystem (e.g., NPP and BDF) changes per area are also linked to strong nitrogen limitation in that system. These basic sensitivity factors provide two relevant axes for frameworks assessing the comparative susceptibility of globally distributed coastal ecosystems to enhanced nitrogen loads, and the effectiveness of mitigation strategies.

The conclusions from above must be tempered by a number of study limitations. First, while the ocean model used in this work has enhanced-resolution relative to most global models and its biogeochemical component is amongst the most comprehensive of those applied to simulate global scale ecosystem changes (Séférian et al., 2020), the resolution remains coarse and biogeochemical processes remain substantially simplified relative to the array of biogeochemical dynamics shaping coastal ecosystems. The most

prominent symptom of these limitations lies in the simulation's inability to capture the intensity of nearshore chlorophyll and PP highs (Figures S3 and S4). While interpretation of these misfits is complicated by the optical complexity of nearshore waters (Schofield et al., 2004), it is a clear model limitation that has been attributed to a combination of limited physical and plankton ecosystem resolution (e.g., Friedrichs et al., 2007; Van Oostende et al., 2018). Previous analysis has demonstrated that model improvements can "sharpen" the representation of nearshore coastal hypoxia (Van Oostende et al., 2018). The complex sedimentary processes, which are of high importance to coastal nutrient budgets and biogeochemical cycles (Middelburg & Levin, 2009; Middelburg et al., 1996, 2007), are also highly parameterized in our model. Because relevant functions in our model were developed primarily for deep waters, we chose to apply certain treatments to account for coastal-specific characteristics. Burial, for example, was first calculated based on Dunne et al. (2007) then ramped upward to its full predicted values with a half-saturation depth of 50 m (i.e., a smaller amount organic detritus was permanently buried in shallower coastal waters). This resulted in a burial term solely as a function of the simulated detrital flux and the ocean depth of that location. Further resolution of the physical and biogeochemical processes that shape these nearshore responses is surely needed to build on the first order factors assessed herein and more fully understand the cross-ecosystem sensitivities to enhanced nitrogen loads.

Other notable caveats tempering the interpretation of results herein are the resolution of dynamic variations in other riverine constituents (e.g., phosphorus and iron), and the limited capacity of our model to simulate phytoplankton responses to nutrient inputs with highly irregular nutrient ratios (Glibert, 2012; Martiny et al., 2013). Although the global patterns of emergent oceanic nutrient limitation in our simulation (Figure S9) agree with nutrient amendment experiments (e.g., Moore et al., 2013) and other global modeling studies (e.g., Deutsch et al., 2007), these limitations may lead to uncertainties at the continental shelf-scales addressed herein. For example, Harrison et al. (1990) conducted mesocosm experiments off the southern coasts of China, suggesting vast but patchy P-limited areas for primary production due to higher-than-Redfield N:P ratios in river waters. This patchiness in nutrient limitation pattern is not sufficiently resolved at our model's resolution (25 km), nor shown in our shelf-scale analysis. An improved understanding of ecosystem responses to river nutrient loads in these areas requires a better resolution of not only limitation factors of phytoplankton growth but also nutrient stoichiometry in river waters. In addition, other processes such as coastal soil erosion (Berhe et al., 2014) and groundwater intrusion (Connolly et al., 2020) that may contribute to changes in coastal nitrogen budgets were not address in our study. We emphasize that enhanced-resolution of phosphorus, iron, and other constituents from rivers, improved parameterizations for key biogeochemical processes in coastal waters and sediments, and improved integration with atmospheric and other nutrient inputs are all important areas for future investigation toward a complete understanding of past and future coastal change (Kim et al., 2011; Raymond & Oh, 2009).

Data Availability Statement

Model outputs used in the analyses and supporting data are openly accessible and archived via Zenodo (https://doi.org/10.5281/zenodo.5142779).

Acknowledgments
This manuscript was prepared by Liu under award NA18OAR4320123 under the Cooperative Institute for Modeling the Earth System (CIMES) at Princeton University, and the National Oceanic and Atmospheric Administration, U.S. Department of Commerce. The statements, findings, conclusions, and recommendations are those of the authors and do not necessarily reflect the views of the National Oceanic and Atmospheric Administration, or the U.S. Department of Commerce. The authors thank J. G. John and J. Y. Park for assistance with model simulations, and J. Luo, and H. G. Lim for comments and suggestions on an earlier draft of this manuscript.

References

Adcroft, A., Anderson, W., Balaji, V., Blanton, C., Bushuk, M., Dufour, C. O., et al. (2019). The GFDL global ocean and sea ice model OM4.0: Model description and simulation features. *Journal of Advances in Modeling Earth Systems*, *11*, 3167–3211. https://doi.org/10.1029/2019ms001726

Antoine, D., & Morel, A. (1996). Oceanic primary production: 1. Adaptation of a spectral light-photosynthesis model in view of application to satellite chlorophyll observations. *Global Biogeochemical Cycles*, *10*, 43–55. https://doi.org/10.1029/95gb02831

Bauer, J. E., Cai, W. J., Raymond, P. A., Bianchi, T. S., Hopkinson, C. S., & Regnier, P. A. G. (2013). The changing carbon cycle of the coastal ocean. *Nature*, *504*(7478), 61–70. https://doi.org/10.1038/nature12857

Berhe, A. A., Arnold, C., Stacy, E., Lever, R., McCorkle, E., & Araya, S. N. (2014). Soil erosion controls on biogeochemical cycling of carbon and nitrogen. *Nature Education Knowledge*, *5*(8), 2.

Blaas, H., & Kroeze, C. (2016). Excessive nitrogen and phosphorus in European rivers: 2000–2050. *Ecological Indicators*, *67*, 328–337. https://doi.org/10.1016/j.ecolind.2016.03.004

Bourgeois, T., Orr, J. C., Resplandy, L., Terhaar, J., Ethe, C., Gehlen, M., & Bopp, L. (2016). Coastal-ocean uptake of anthropogenic carbon. *Biogeosciences*, *13*(14), 4167–4185. https://doi.org/10.5194/bg-13-4167-2016

Bouwman, A. F., Kram, T., & Klein Goldewijk, K. (2006). *Integrated modelling of global environmental change. An overview of IMAGE 2.4* (p. 228). Netherlands Environmental Assessment Agency.

Bouwman, L., Goldewijk, K. K., Van Der Hoek, K. W., Beusen, A. H., Van Vuuren, D. P., Willems, J., et al. (2013). Exploring global changes in nitrogen and phosphorus cycles in agriculture induced by livestock production over the 1900–2050 period. *Proceedings of the National Academy of Sciences*, *110*(52), 20882–20887. https://doi.org/10.1073/pnas.1012878108

Cahill, B., Wilkin, J., Fennel, K., Vandemark, D., & Friedrichs, M. A. M. (2016). Interannual and seasonal variabilities in air-sea CO_2 fluxes along the US eastern continental shelf and their sensitivity to increasing air temperatures and variable winds. *Journal of Geophysical Research: Biogeosciences*, *121*(2), 295–311. https://doi.org/10.1002/2015jg002939

Cai, W. J. (2011). Estuarine and coastal ocean carbon paradox: CO_2 sinks or sites of terrestrial carbon incineration? *Annual Review of Marine Science*, *3*, 123–145. https://doi.org/10.1146/annurev-marine-120709-142723

Cloern, J. E. (1999). The relative importance of light and nutrient limitation of phytoplankton growth: A simple index of coastal ecosystem sensitivity to nutrient enrichment. *Aquatic Ecology*, *33*, 3–15. https://doi.org/10.1023/A:1009952125558

Connolly, C. T., Cardenas, M. B., Burkart, G. A., Spencer, R. G. M., & McClelland, J. W. (2020). Groundwater as a major source of dissolved organic matter to Arctic coastal waters. *Nature Communications*, *11*, 1479. https://doi.org/10.1038/s41467-020-15250-8

Dagg, M., & Breed, G. (2003) Biological effects of Mississippi River nitrogen on the northern gulf of Mexico—A review and synthesis. *Journal of Marine Systems 43*(3–4), 133–152. https://doi.org/10.1016/j.jmarsys.2003.09.002

de Mutsert, K., Steenbeek, J., Lewis, K., Buszowski, J., Cowan, J. H., & Christensen, V. (2016). Exploring effects of hypoxia on fish and fisheries in the northern Gulf of Mexico using a dynamic spatially explicit ecosystem model. *Ecological Modelling*, *331*, 142–150. https://doi.org/10.1016/j.ecolmodel.2015.10.013

Deutsch, C., Sarmiento, J., Sigman, D., Gruber, N., & Dunne, J. P. (2007). Spatial coupling of nitrogen inputs and losses in the ocean. *Nature*, *445*, 163–167. https://doi.org/10.1038/nature05392

Diaz, R. J., & Rosenberg, R. (2008). Spreading dead zones and consequences for marine ecosystems. *Science*, *321*(5891), 926–929. https://doi.org/10.1126/science.1156401

Doney, S. C. (2010). The growing human footprint on coastal and open-ocean biogeochemistry. *Science*, *328*(5985), 1512–1516. https://doi.org/10.1126/science.1185198

Dunne, J. P., Hales, B., & Toggweiler, J. R. (2012). Global calcite cycling constrained by sediment preservation controls. *Global Biogeochemical Cycles*, *26*(3). https://doi.org/10.1029/2010GB003935

Dunne, J. P., Sarmiento, J. L., & Gnanadesikan, A. (2007). A synthesis of global particle export from the surface ocean and cycling through the ocean interior and on the seafloor. *Global Biogeochemical Cycles*, *21*(4). https://doi.org/10.1029/2006GB002907

Feng, Y., Friedrichs, M. A. M., Wilkin, J., Tian, H., Yang, Q., Hofmann, E. E., et al. (2015). Chesapeake Bay nitrogen fluxes derived from a land-estuarine ocean biogeochemical modeling system: Model description, evaluation, and nitrogen budgets. *Journal of Geophysical Research: Biogeosciences*, *120*, 1666–1695. https://doi.org/10.1002/2015JG002931

Fennel, K., & Laurent, A. (2018). N and P as ultimate and proximate limiting nutrients in the northern Gulf of Mexico: Implications for hypoxia reduction strategies. *Biogeosciences*, *15*, 3121–3131. https://doi.org/10.5194/bg-15-3121-2018

Fennel, K., & Testa, J. M. (2019). Biogeochemical controls on coastal hypoxia. *Annual Review of Marine Science*, *11*, 105–130. https://doi.org/10.1146/annurev-marine-010318-095138

Fennel, K., Wilkin, J., Previdi, M., & Najjar, R. (2008). Denitrification effects on air-sea CO_2 flux in the coastal ocean: Simulations for the northwest North Atlantic. *Geophysical Research Letters*, *35*(24). https://doi.org/10.1029/2008gl036147

Friedrichs, M. A. M., Dusenberry, J. A., Anderson, L. A., Armstrong, R. A., Chai, F., Christian, J. R., et al. (2007). Assessment of skill and portability in regional marine biogeochemical models: Role of multiple planktonic groups. *Journal of Geophysical Research*, *112*(C8). https://doi.org/10.1029/2006JC003852

Friedrichs, M. A. M., St-Laurent, P., Xiao, Y. J., Hofmann, E., Hyde, K., ManninoNajjar, A. R. G., et al. (2019). Ocean circulation causes strong variability in the Mid-Atlantic Bight nitrogen budget. *Journal of Geophysical Research-Oceans*, *124*(1), 113–134. https://doi.org/10.1029/2018jc014424

Garcia, H. E., Locarnini, R. A., Boyer, T. P., Antonov, J. I., Baranova, O. K., Zweng, M. M., et al. (2014a). World ocean atlas 2013, Volume 3: Dissolved oxygen, apparent oxygen utilization, and oxygen saturation. In S. Levitus, & A. Mishonov (Eds.), *NOAA Atlas NESDIS* (Vol. 75, p. 27).

Garcia, H. E., Locarnini, R. A., Boyer, T. P., Antonov, J. I., Baranova, O. K., Zweng, M. M., et al. (2014b). World ocean atlas 2013, Volume 4: Dissolved inorganic nutrients (phosphate, nitrate, silicate). In S. Levitus, & A. Mishonov (Eds.), *NOAA Atlas NESDIS* (Vol. 76, p. 25).

Garcia, H. E., Weathers, K., Paver, C. R., Smolyar, I., Boyer, T. P., Locarnini, R. A., et al. (2018). World ocean atlas 2018, Volume 4: Dissolved inorganic nutrients (phosphate, nitrate and nitrate+nitrite, silicate). In A. Mishonov (Ed.), *NOAA Atlas NESDIS* (Vol. 84, p. 35).

Gerber, S., Hedin, L. O., Oppenheimer, M., Pacala, S. W., & Shevliakova, E. (2010). Nitrogen cycling and feedbacks in a global dynamic land model. *Global Biogeochemical Cycles*, *24*(1). https://doi.org/10.1029/2008GB003336

Gilbert, D., Rabalais, N. N., Diaz, R. J., & Zhang, J. (2010). Evidence for greater oxygen decline rates in the coastal ocean than in the open ocean. *Biogeosciences*, *7*(7), 2283–2296. https://doi.org/10.5194/bg-7-2283-2010

Glibert, P. M. (2012). Ecological stoichiometry and its implications for aquatic ecosystem sustainability. *Current Opinion in Environmental Sustainability*, *4*, 272–277.

Green, P. A., Vörösmarty, C. J., Meybeck, M., Galloway, J. N., Peterson, B. J., & Boyer, E. W. (2004). Pre-industrial and contemporary fluxes of nitrogen through rivers A global assessment based on topology. *Biogeochemistry*, *68*, 71–105. https://doi.org/10.1023/b:biog.0000025742.82155.92

Harrison, P. J., Hu, M. H., Yang, Y. P., & Lu, X. (1990). Phosphate limitation in estuarine and coastal waters of China. *Journal of Experimental Marine Biology and Ecology*, *140*(1–2), 79–87. https://doi.org/10.1016/0022-0981(90)90083-o

Herbert, R. A. (1999). Nitrogen cycling in coastal marine ecosystems. *FEMS Microbiology Reviews*, *23*(5), 563–590. https://doi.org/10.1111/j.1574-6976.1999.tb00414.x

Holt, J., Hyder, P., Ashworth, M., Harle, J., Hewitt, H. T., Liu, H., et al. (2017). Prospects for improving the representation of coastal and shelf seas in global ocean models. *Geoscientific Model Development*, *10*(1), 499–523. https://doi.org/10.5194/gmd-10-499-2017

Horowitz, L. W. (2006). Past, present, and future concentrations of tropospheric ozone and aerosols: Methodology, ozone evaluation, and sensitivity to aerosol wet removal. *Journal of Geophysical Research: Atmospheres*, *111*(D22). https://doi.org/10.1029/2005jd006937

Howarth, R. W., & Marino, R. (2006). Nitrogen as the limiting nutrient for eutrophication in coastal marine ecosystems: Evolving views over three decades. *Limnology and Oceanography*, *51*(1 part 2), 364–376. https://doi.org/10.4319/lo.2006.51.1_part_2.0364

Howarth, R. W., Marino, R., & Cole, J. J. (1988). Nitrogen fixation in freshwater, estuarine, and marine ecosystems. 1. Biogeochemical controls. *Limnology and Oceanography*, *33*, 688–701. https://doi.org/10.4319/lo.1988.33.4part2.0688

IPCC. (2019). In P. R. Shukla, J. Skea, E. Calvo Buendia, V. Masson-Delmotte, H.-O. Pörtner, D. C. Roberts, et al. (Eds.), *Climate change and land: An IPCC special report on climate change, desertification, land degradation, sustainable land management, food security, and greenhouse gas fluxes in terrestrial ecosystems*.

Izett, J. G., & Fennel, K. (2018). Estimating the cross-shelf export of riverine materials: Part 2. Estimates of global freshwater and nutrient export. *Global Biogeochemical Cycles*, *32*, 176–186. https://doi.org/10.1002/2017GB005668

Kim, T.-W., Lee, K., Najjar, R. G., Jeong, H.-D., & Jeong, H. J. (2011). Increasing N abundance in the northwestern Pacific Ocean due to atmospheric nitrogen deposition. *Science*, *334*(6055), 505–509. https://doi.org/10.1126/science.1206583

Lee, M., Malyshev, S., Shevliakova, E., Milly, P. C. D., & Jaffe, P. R. (2014). Capturing interactions between nitrogen and hydrological cycles under historical climate and land use: Susquehanna watershed analysis with the GFDL land model LM3-TAN. *Biogeosciences*, *11*(20), 5809–5826. https://doi.org/10.5194/bg-11-5809-2014

Lee, M., Shevliakova, E., Stock, C. A., Malyshev, S., & Milly, P. C. D. (2019). Prominence of the tropics in the recent rise of global nitrogen pollution. *Nature Communications*, *10*. https://doi.org/10.1038/s41467-019-09468-4

Liu, S. M., Zhang, J., Chen, H. T., & Zhang, G. S. (2005). Factors influencing nutrient dynamics in the eutrophic Jiaozhou Bay, North China. *Progress in Oceanography*, *66*, 66–85. https://doi.org/10.1016/j.pocean.2005.03.009

Liu, X., Dunne, J. P., Stock, C. A., Harrison, M. J., Adcroft, A., & Resplandy, L. (2019). Simulating water residence time in the coastal ocean: A global perspective. *Geophysical Research Letters*, *46*, 13910–13919. https://doi.org/10.1029/2019gl085097

Locarnini, R. A., Mishonov, A. V., Antonov, J. I., Boyer, T. P., Garcia, H. E., Baranova, O. K., et al. (2013). World ocean atlas 2013, Volume 1: Temperature. In S. Levitus, & A. Mishonov (Eds.), *NOAA Atlas NESDIS* (Vol. 73, p. 40).

Lotze, H. K., Lenihan, H. S., Bourque, B. J., Bradbury, R. H., Cooke, R. G., Kay, M. C., et al. (2006). Depletion, degradation, and recovery potential of estuaries and coastal seas. *Science*, *312*(5781), 1806–1809. https://doi.org/10.1126/science.1128035

Lu, C., & Tian, H. (2017). Global nitrogen and phosphorus fertilizer use for agriculture production in the past half century: Shifted hot spots and nutrient imbalance. *Earth System Science Data*, *9*, 181–192. https://doi.org/10.5194/essd-9-181-2017

Maritorena, S., Hembise Fanton d'Andon, O., Mangin, A., & Siegel, D. A. (2010). Merged satellite ocean color data products using a bio-optical model: Characteristics, benefits and issues. *Remote Sensing of Environment*, *114*(8), 1791–1804. https://doi.org/10.1016/j.rse.2010.04.002

Martiny, A., Pham, C., Primeau, F., Vrugt, J. A., Moore, J. K., Levin, S. A., & Lomas, M. W. (2013). Strong latitudinal patterns in the elemental ratios of marine plankton and organic matter. *Nature Geoscience*, *6*, 279–283. https://doi.org/10.1038/ngeo1757

Middelburg, J. J., & Levin, L. A. (2009). Coastal hypoxia and sediment biogeochemistry. *Biogeosciences*, *6*, 1273–1293. https://doi.org/10.5194/bg-6-1273-2009

Middelburg, J. J., Soetaert, K., Herman, P. M., Boschker, H. T., & Heip, C. H. (2007). Burial of nutrient in coastal sediments: The role of primary producers. *Estuarine nutrient cycling: The influence of primary producers* (pp. 217–230). Springer.

Middelburg, J. J., Soetaert, K., Herman, P. M. J., & Heip, C. H. R. (1996). Denitrification in marine sediments: A model study. *Global Biogeochemical Cycles*, *10*(4), 661–673. https://doi.org/10.1029/96GB02562

Milly, P. C., Malyshev, S. L., Shevliakova, E., Dunne, K. A., Findell, K. L., Gleeson, T., et al. (2014). An enhanced model of land water and energy for global hydrologic and earth-system studies. *Journal of Hydrometeorology*, *15*, 1739–1761. https://doi.org/10.1175/JHM-D-13-0162.1

Moore, C., Mills, M., Arrigo, K., Berman-Frank, I., Bopp, L., Boyd, P. W., et al. (2013). Processes and patterns of oceanic nutrient limitation. *Nature Geoscience*, *6*, 701–710. https://doi.org/10.1038/ngeo1765

Murray, C., Müller-Karulis, B., Carstensen, J., Conley, D. J., Gustafsson, B., & Andersen, J. H. (2019). Past, present and future eutrophication status of the Baltic Sea. *Frontiers in Marine Science*, *6*, 2. https://doi.org/10.3389/fmars.2019.00002

Najjar, R. G., Herrmann, M., Alexander, R., Boyer, E. W., Burdige, D. J., Butman, D., et al. (2018). Carbon budget of tidal wetlands, estuaries, and shelf waters of Eastern North America. *Global Biogeochemical Cycles*, *32*(3), 389–416. https://doi.org/10.1002/2017gb005790

Olsen, A., Key, R. M., van Heuven, S., Lauvset, S. K., Velo, A., Lin, X., et al. (2016). The Global Ocean Data Analysis Project version 2 (GLODAPv2) – An internally consistent data product for the world ocean. *Earth System Science Data*, *8*, 297–323. https://doi.org/10.5194/essd-8-297-2016

Orr, J. C., Fabry, V. J., Aumont, O., Bopp, L., Doney, S. C., Feely, R. A., et al. (2005). Anthropogenic ocean acidification over the twenty-first century and its impact on calcifying organisms. *Nature*, *437*(7059), 681–686. https://doi.org/10.1038/nature04095

Paerl, H. W., Otten, T. G., & Kudela, R. (2018). Mitigating the expansion of harmful algal blooms across the freshwater-to-marine continuum. *Environmental Science and Technology*, *52*, 5519–5529. https://doi.org/10.1021/acs.est.7b05950

Pauly, D., & Zeller, D. (2016). Catch reconstructions reveal that global marine fisheries catches are higher than reported and declining. *Nature Communications*, *7*, 10244. https://doi.org/10.1038/ncomms10244

Pitcher, G. C., Figueiras, F. G., Hickey, B. M., & Moita, M. T. (2010). The physical oceanography of upwelling systems and the development of harmful algal blooms. *Progress in Oceanography*, *85*, 5–32. https://doi.org/10.1016/j.pocean.2010.02.002

Rabalais, N. N., Turner, R. E., Diaz, R. J., & Justic, D. (2009). Global change and eutrophication of coastal waters. *ICES Journal of Marine Science*, *66*(7), 1528–1537. https://doi.org/10.1093/icesjms/fsp047

Raymond, P. A., & Oh, N.-H. (2009). Long term changes of chemical weathering products in rivers heavily impacted from acid mine drainage: Insights on the impact of coal mining on regional and global carbon and sulfur budgets. *Earth and Planetary Science Letters*, *284*(1–2), 50–56. https://doi.org/10.1016/j.epsl.2009.04.006

Regnier, P., Friedlingstein, P., Ciais, P., Mackenzie, F. T., Gruber, N., Janssens, I. A., et al. (2013). Anthropogenic perturbation of the carbon fluxes from land to ocean. *Nature Geoscience*, *6*(8), 597–607. https://doi.org/10.1038/ngeo1830

Schofield, O., Arnone, R. A., Bissett, W. P., Dickey, T. D., Davis, C. O., Finkel, Z., et al. (2004). Watercolors in the coastal zone: What can we see? *Oceanography*, *17*, 24–31. https://doi.org/10.5670/oceanog.2004.44

Séférian, R., Berthet, S., Yool, A., Palmiéri, J., Bopp, L., Tagliabue, A., et al. (2020). Tracking improvement in simulated marine biogeochemistry between CMIP5 and CMIP6. *Current Climate Change Reports*, *6*, 95–119. https://doi.org/10.1007/s40641-020-00160-0

Seitzinger, S. P., Harrison, J. A., Böhlke, J. K., Bouwman, A. F., Lowrance, R., Peterson, B., et al. (2006). Denitrification across landscapes and waterscapes: A synthesis. *Ecological Applications*, *16*(6), 2064–2090. https://doi.org/10.1890/1051-0761(2006)016[2064:dalawa]2.0.co;2

Seitzinger, S. P., Harrison, J. A., Dumont, E., Beusen, A. H. W., & Bouwman, A. F. (2005). Sources and delivery of carbon, nitrogen, and phosphorus to the coastal zone: An overview of Global Nutrient Export from Watersheds (NEWS) models and their application. *Global Biogeochemical Cycles*, *19*(4). https://doi.org/10.1029/2005GB002606

Seitzinger, S. P., Kroeze, C., Bouwman, A. F., Caraco, N., Dentener, F., & Styles, R. V. (2002). Global patterns of dissolved inorganic and particulate nitrogen inputs to coastal systems: Recent conditions and future projections. *Estuaries*, *25*(4b), 640–655. https://doi.org/10.1007/bf02804897

Seitzinger, S. P., Mayorga, E., Bouwman, A. F., Kroeze, C., Beusen, A. H. W., Billen, G., et al. (2010). Global river nutrient export: A scenario analysis of past and future trends. *Global Biogeochemical Cycles*, *24*(4). https://doi.org/10.1029/2009GB003587

Sharples, J., Middelburg, J. J., Fennel, K., & Jickells, T. D. (2017). What proportion of riverine nutrients reaches the open ocean? *Global Biogeochemical Cycles*, *31*, 39–58. https://doi.org/10.1002/2016GB005483

Shevliakova, E., Pacala, S. W., Malyshev, S., D Milly, P. C., Sentman, L. T., Caspersen, J. P., et al. (2009). Carbon cycling under 300 years of land use change: Importance of the secondary vegetation sink. *Global Biogeochemical Cycles*, *23*(2). https://doi.org/10.1029/2007GB003176

Stock, C. A., Dunne, J. P., Fan, S., Ginoux, P., John, J., Krasting, J., et al. (2020). Ocean biogeochemistry in GFDL's Earth System Model 4.1 and its response to increasing atmospheric CO_2. *Journal of Advances in Modeling Earth Systems*, *12*, e2019MS002043. https://doi.org/10.1029/2019ms002043

Stock, C. A., Jasmin, G. J., Rykaczewski, R. R., Asch, R. G., Cheung, W. W. L., Dunne, J. P., et al. (2017). Reconciling fisheries catch and ocean productivity. *Proceedings of the National Academy of Sciences*, *114*(8), E1441–E1449. https://doi.org/10.1073/pnas.1610238114

Teichberg, M., Fox, S. E., Olsen, Y. S., Valiela, I., Martinetto, P., Iribarne, O., et al. (2010). Eutrophication and macroalgal blooms in temperate and tropical coastal waters: Nutrient enrichment experiments with Ulva spp. *Global Change Biology*, *16*, 2624–2637. https://doi.org/10.1111/j.1365-2486.2009.02108.x

Tsujino, H., Urakawa, S., Nakano, H., Small, R., Kim, W., Yeager, S., et al. (2018). JRA-55 based surface dataset for driving ocean–sea-ice models (JRA55-do). *Ocean Modelling*, *130*, 79–139. https://doi.org/10.1016/j.ocemod.2018.07.002

Van Oostende, N., Dussin, R., Stock, C. A., Barton, A. D., Curchitser, E., Dunne, J. P., & Ward, B. B. (2018). Simulating the ocean's chlorophyll dynamic range from coastal upwelling to oligotrophy. *Progress in Oceanography*, *168*, 232–247. https://doi.org/10.1016/j.pocean.2018.10.009

Voss, M., Bange, H. W., Dippner, J. W., Middelburg, J. J., Montoya, J. P., & Ward, B. (2013). The marine nitrogen cycle: Recent discoveries, uncertainties and the potential relevance of climate change. *Philosophical Transactions of the Royal Society B: Biological Sciences*, *368*, 20130121. https://doi.org/10.1098/rstb.2013.0121

Wiegner, T. N., Seitzinger, S. P., Glibert, P. M., & Bronk, D. A. (2006). Bioavailability of dissolved organic nitrogen and carbon from nine rivers in the eastern United States. *Aquatic Microbial Ecology*, *43*, 277–287. https://doi.org/10.3354/ame043277

Worm, B., Barbier, E. B., Beaumont, N., Duffy, J. E., Folke, C., Halpern, B. S., et al. (2006). Impacts of biodiversity loss on ocean ecosystem services. *Science*, *314*(5800), 787–790. https://doi.org/10.1126/science.1132294

Zhang, J., Shi, J., Gao, S., Huo, Y., Cui, J., Shen, H., et al. (2019). Annual patterns of macroalgal blooms in the Yellow Sea during 2007–2017. *PloS One*, *14*(1), e0210460. https://doi.org/10.1371/journal.pone.0210460

Zweng, M. M., Reagan, J. R., Antonov, J. I., Locarnini, R. A., Mishonov, A. V., Boyer, T. P., et al. (2013). World ocean atlas 2013, Volume 2: Salinity. In S. Levitus, & A. Mishonov (Eds.), *NOAA Atlas NESDIS* (Vol. 74, p. 39).